New robust coil sensors for near field characterization

Benjamin Vincent, Olivier Chadebec, Jean-Luc Schanen, Carlos Antonio França Sartori, Laurent Krähenbühl, Ronan Perrussel, Kévin Berger

New robust coil sensors for near field characterization

B. Vincent[1], O. Chadebec[1] , J.-L. Schanen[1], C.A.F. Sartori[2]
L. Krähenbühl[2, 3], R. Perrussel[3], K. Berger[3]

(1) Grenoble Electrical Engineering Lab (G2Elab, CNRS UMR5269)
INPG-UJF, ENSIEG, BP 46, 38402 Grenoble, France
(2) Escola Politécnica da Universidade de São Paulo (Lmag/PEA-EPUSP), 05508-900 São Paulo, SP, Brasil
(3) Ampère (CNRS UMR5005), Université de Lyon, Ecole Centrale de Lyon, 69134 Ecully CEDEX, France.

***Abstract*— This work introduces a new generation of magnetic field sensors, based on the spherical harmonic decomposition concept. The measurement principle is similar to a spatial filtering: according to the coil shape, the sensors are just sensitive to a specific component of the multipolar expansion. Five coil shapes are determined, in order to account for the first two orders of the multipolar expansion. The way of determining the coil shape is first explained, and a validation is proposed using a finite element software.**

***Index Terms*—** Coils electromagnetic sensors; near field measurements; multipolar expansion; radiated EMC; radiated electromagnetic sources characterization.

I. INTRODUCTION

With the increase of power density in modern power systems, interactions between various elements become a key point to be addressed. This problem can be handled at various scales: interactions between two variable speed drives or power transformers in the same room ("indoor EMC"), interactions between power and the control board, or between different devices on the same board. On this latter example, magnetic couplings between magnetic components (inductor, transformer) and/or wires are often encountered and may lead to dysfunctions or a bad filtering.

Addressing these magnetic couplings implies to have the ability to characterize the magnetic field close to the sources. The whole knowledge of this near field can be achieved using simulation or experimentation.

The first idea starts from a simple mapping of the near magnetic field, using some magnetic sensors and sampling the space by moving the sensors around the system, by moving the system itself, by increasing the number of sensors, or by using any appropriate combination of all previous solutions.

After this step, the magnetic field is characterized by a set of thousands of measurements. These data must therefore be summarized into a simpler equivalent source in order to make possible the study of interactions.

One method to describe equivalent sources is the multipolar expansion, which has previously

shown its ability to synthesize any magnetic source into known standardized sources (dipole, quadrupole, etc.). For instance, it has been shown that a set of several thousands of data points can be summarized into 15 terms, with a large validity region [1].

However, the post-processing of punctual measurements to obtain the coefficients of the multipolar expansion leads to inaccuracies, either due to measurement errors or due to mechanical positioning errors [2], [3].

The present work tackles particular sensors, which are sensitive to a specific component of the multipolar expansion. The principle is based on the measurement of the magnetic flux through large coils placed around the device. These coils are used to achieve a spatial integration and consequently to reduce positioning inaccuracies [3]-[5]. As an example, to measure the first order of the decomposition (dipole), the Standard CISPR 16-1 [6], proposes using three orthogonal loops (Fig. 1). This standard applies for the medium frequency range: 9 kHz to 30 MHz.

The problem is that no source is composed of pure dipoles. Therefore, even the standard method leads to errors. For the sensor design, we propose to take into account higher order terms in the expansion, and to improve the selectivity property, as proposed initially in [7].

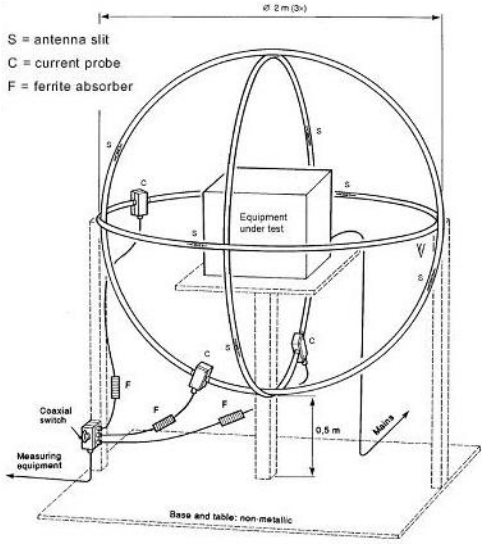

Fig. 1. From Standard CISPR 16-1, the loop-antenna system, consisting in three perpendicular large loop-antennas.

The mathematical model of the equivalent sources is first recalled. The design of the sensor geometry can then be detailed and validated by a finite element model of an actual device.

II. MULTIPOLAR EXPANSION

The multipolar expansion is a classical tool used for electromagnetic field representation [8], [9]. It allows decomposing any field into an infinite sum of simple terms. The first order of the decomposition is the well known dipole. Several mathematical basis functions can be used for the decomposition. For near field studies, the quasi-static approximation is suitable i.e. displacement currents can be neglected. Therefore, the basis does not include propagation terms [8]. Near field area is limited by $\lambda/6$ meters. According to the maximum frequency, quasi static approximation is

available up to 1.7 meter.

A.Time and space harmonic decompositions

Outside a sphere including all radiation sources, the magnetic field can be completely described by a magnetic scalar potential $\psi(t)$. This potential is solution of the Laplace equation:

$$\Delta\psi(t) = 0 \tag{1}$$

We consider the harmonic decomposition of time varying sources. Each term of the harmonic decomposition of the time varying solution of (1) can be expressed as follows:

$$\begin{cases} \Psi(r,\theta,\varphi) = \sum_{n=1}^{+\infty}\sum_{m=-n}^{+n} A_{nm}\cdot\frac{1}{r^{n+1}}\cdot Y_{nm}(\theta,\varphi) \\ \mathbf{B}(r,\theta,\varphi) = -\mathbf{grad}(\Psi) \\ \mathbf{B}(r,\theta,\varphi) = \sum_{n=1}^{+\infty}\sum_{m=-n}^{+n}\mathbf{B}_{nm} \end{cases} \tag{2}$$

where:

- Y_{nm} are the spherical harmonics of order n,
- r, the distance between the center of the decomposition and the point where the field is expressed,
- $\mathbf{B}_{nm}$, the elementary magnetic fields of the decomposition,
- A_{nm}, the coefficients of the decomposition, i.e. the unknowns.

B.Relevance

The choice of this multipolar expansion is mainly motivated by the $r^{-(n+1)}$ decrease of the terms of order n. This insures a hierarchy between each order of the decomposition. The larger the distance to the source is, the fewer are the terms required to reconstruct the field.

For interaction studies, we have decided to limit the expansion to the two first orders of the decomposition. This also corresponds to the physical behavior of most sources in electrical systems, where disturbances often originate from current loops. Therefore, the number of unknowns is limited to only 8 (from (2), there are $2n+1$ coefficients for each order n; thus, 3 unknowns for order 1 and 5 for order 2).

The aim of the identification is to deduce these 8 unknowns from measurements achieved around the radiation source. For this purpose, one possible solution is to take advantage of the fast decrease of the high order terms with the distance: far from the source, the sensors are only sensitive to the dipole. This property has been used in Standard CISPR16-1 [4]-[7]. This leads to large measurement systems, and furthermore, the accuracy is poor: far from the Device Under Test (DUT), the field is low, and the signal is small. Furthermore, the size implies frequency limitations: it is difficult to reach 30 MHz without accounting for propagation effects. Instead of taking advantage of the $r^{-(n+1)}$ behavior only, our design strategy, introduced in the next section, is to use the geometrical properties of the spherical harmonic functions Y_{nm}.

III. SENSOR DESIGN

A. Preliminaries

Each component sensor, dedicated to a specific component of the multipolar expansion is constituted of several coils. They are located on a sphere S_M, with a radius r_0, including the validity sphere region. An example is shown in Fig. 2.

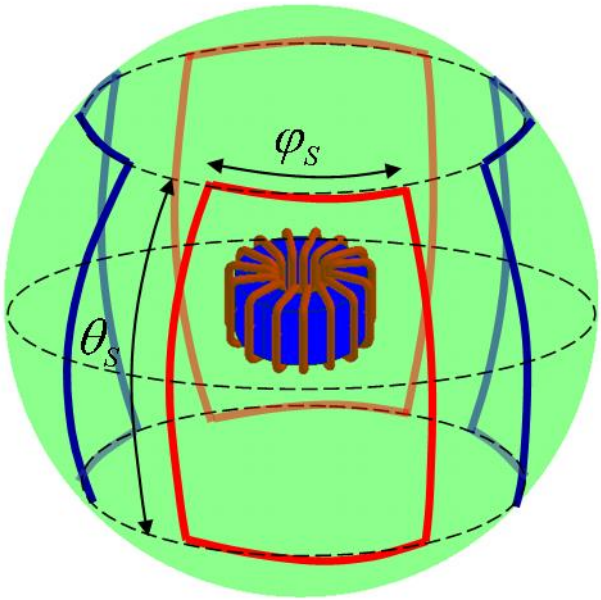

Fig. 2. An example of a component sensor located on sphere S_M and centered on the Device Under Test. The sensor is composed of several coils defined by angles θ_S and φ_S.

The principle consists in measuring the magnetic flux through the coils. As a component sensor is constituted of several coils, it is possible to compose all flux (sum or difference). The following representation will be used in this paper: a red coil will correspond to a positive outgoing flux, whereas a blue one will correspond to a negative outgoing flux (see Fig. 2 for example).

Any set of coils on the sphere S_M can then be represented by a "sensor function" M defined by:

- $M(\theta,\varphi) = 1$ for a portion of S_M delimited by a red coil,
- $M(\theta,\varphi) = -1$ for a portion of S_M delimited by a blue coil,
- $M(\theta,\varphi) = 0$ for the remaining S_M area.

The measurement corresponds to:

$$Flux = \iint_{S_M} M(\theta,\varphi)\,\mathbf{B}(r_0,\theta,\varphi)\cdot\mathbf{n}\,dS = \iint_{S_M} M(\theta,\varphi)\,B_r(r_0,\theta,\varphi)\,dS \tag{3}$$

where $\boldsymbol{n}$ is the unit outgoing normal of S_M and $B_r(r_0,\theta,\varphi)$ the radial component of the induction on S_M, defined by:

$$B_r(r_0,\theta,\varphi) = \sum_{n=1}^{+\infty}\sum_{m=-n}^{+n} \frac{(n+1)}{r_0^{n+2}} A_{nm} Y_{nm}(\theta,\varphi) \tag{4}$$

The ideal sensor would be sensitive to a single component of (4). We will show that it cannot be realized but, if the decomposition in (4) is truncated to n = 4, solutions exist. Consequently, the most complex multipolar field created by the source is limited to the 4th order (24 components) in our

study. It has been considered sufficient for most of practical power electronic radiating systems.

In the following, let n and m denote the indices of the component $\mathbf{B}_{nm}$ to identify and M_{nm} the "sensor function" dedicated to $\mathbf{B}_{nm}$. Indices n' and m' will be used for the other components which can create a parasitic flux. This disturbance flux will have to be cancelled by sensor function M_{nm}. The problem can be written as:

$$\begin{aligned} Flux_{nm} &= \iint_{S_M} M_{nm}(\theta,\varphi) \sum_{n'=1}^{+4} \sum_{m'=-n'}^{+n'} \frac{(n'+1)}{r_0^{n'+2}} A_{n'm'} Y_{n'm'}(\theta,\varphi)\, dS = \sum_{n'=1}^{+4} \sum_{m'=-n'}^{+n'} \frac{(n'+1)}{r_0^{n'+2}} A_{n'm'} \iint_{S_M} M_{nm}(\theta,\varphi) Y_{n'm'}(\theta,\varphi)\, dS \\ &= \frac{(n+1)}{r_0^{n+2}} A_{nm} \iint_{S_M} M_{nm}(\theta,\varphi) Y_{nm}(\theta,\varphi)\, dS \end{aligned} \tag{5}$$

Thus, we have to design, for each component, a function M_{nm} such as:

$$\iint_{S_M} M_{nm}(\theta,\varphi) Y_{n'm'}(\theta,\varphi)\, dS = 0, \quad \forall (n',m') \neq (n,m) \tag{6}$$

In other words, the goal is to accomplish a spatial filtering of B_r (24 components) thanks to functions sensors M_{nm} (8 sensors for the first 8 components). Equation (5) shows us that the measurement of flux allows an efficient identification of coefficients A_{nm}. Moreover, we can see that the field distribution on sphere S_M is directly linked to the characteristics of functions Y_{nm}. Their study is therefore sufficient for finding M_{nm}.

B. Behavior of functions Y_{nm}

The real spherical harmonic function of order n and degree m is given by (7):

$$Y_{nm} = \Theta_{nm}(\theta).\Phi_m(\varphi)$$

$$\text{where,} \qquad \Theta_{nm}(\theta) = \sqrt{\frac{(n-|m|)!}{(n+|m|)!}} P_{n|m|}(\cos(\theta)) \tag{7}$$

$$\Phi_m(\varphi) = \begin{cases} \sqrt{2}\cos(m\varphi) & m > 0 \\ 1 \quad \text{if} & m = 0 \\ \sqrt{2}\sin(|m|\varphi) & m < 0 \end{cases}$$

The P_{nm} are the Legendre polynomials defined thanks to Rodrigues formulae [10].

From (7), we can deduce that:

$$Y_{n,-m}(\theta,\varphi) = -Y_{nm}(\theta,\varphi + \pi/2m) \tag{8}$$

The only difference between Y_{nm} and $Y_{n,-m}$ is a rotation of $\pi/2m$ around z axis. The study can therefore be limited, for each order n, to the cases $m \geq 0$. The 8 sensor shapes can be reduced to 5 (2 for $n = 1$ and 3 for $n = 2$). Functions Y_{nm} are presented on Fig. 3 for the four first orders.

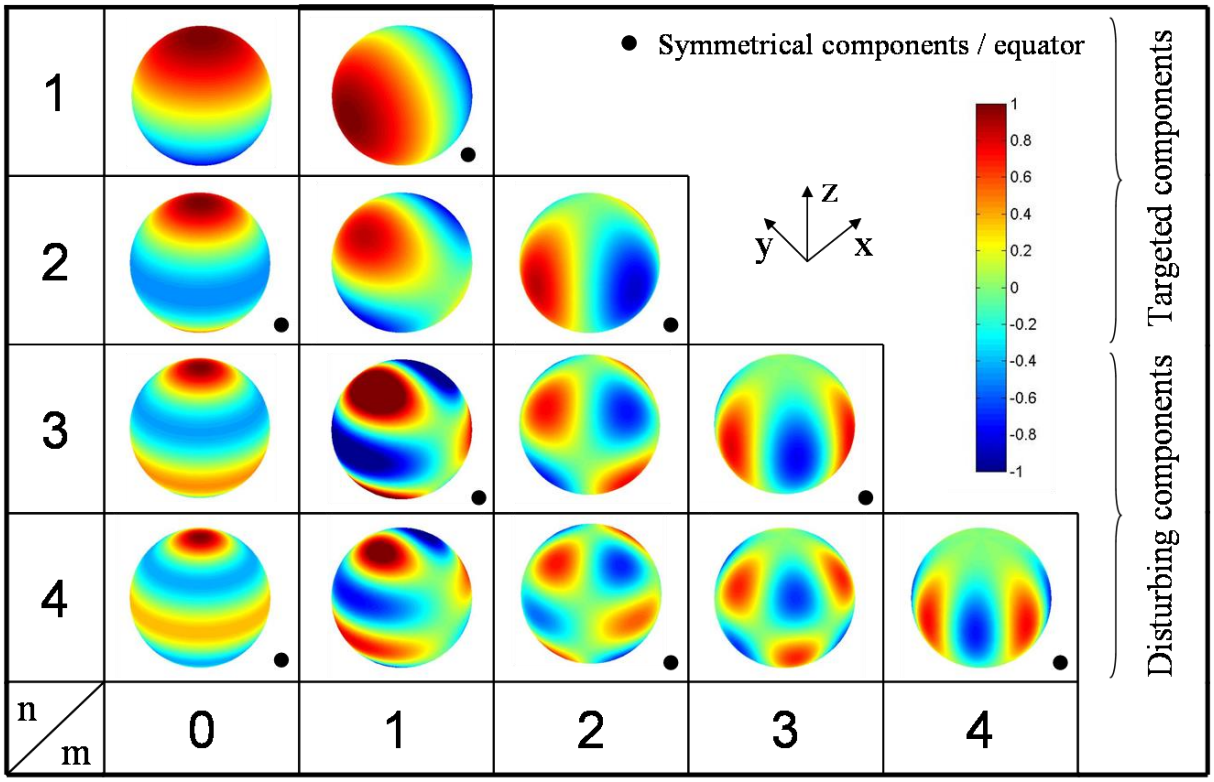

Fig. 3. Spherical harmonic functions of the reference source for $n \le 4$ and $m \ge 0$.

To simplify the coil design process, their shapes will be chosen with constant θ or φ angles, i.e. these coils will follow only meridians or parallels of the sphere. This design constraint is suggested by (7) where the function Y_{nm} depends separately on θ and φ variables. Therefore, function M_{nm} can be written as:

$$M_{nm}(\theta,\varphi) = M_{nm}^{\theta}(\theta).M_{nm}^{\varphi}(\varphi) \tag{9}$$

Thus, the design method can separately study geometrical characteristics of functions $\Theta_{n'm'}$ and $\Phi_{m'}$. Indeed, according to (7) and (9), (5) is equivalent to:

$$\begin{aligned} Flux_{nm} &= \sum_{n'=1}^{+4}\sum_{m'=-n'}^{+n'} \frac{(n'+1)}{r_0^{n'+2}} A_{nm}\left(\int_{\theta=0}^{\pi} M_{nm}^{\theta}(\theta).\Theta_{n'm'}(\theta)\sin(\theta)\,d\theta\right)\left(\int_{\varphi=0}^{2\pi} M_{nm}^{\varphi}(\varphi).\Phi_{m'}(\varphi)\,d\varphi\right) \\ &\propto A_{nm}\left(\int_{\theta=0}^{\pi} M_{nm}^{\theta}(\theta).\Theta_{nm}(\theta)\sin(\theta)\,d\theta\right)\left(\int_{\varphi=0}^{2\pi} M_{nm}^{\varphi}(\varphi).\Phi_{m}(\varphi)\,d\varphi\right) \end{aligned} \tag{10}$$

Last, according to (10) and (6), the problem can be summarized by:

$$\left(\int_{\theta=0}^{\pi} M_{nm}^{\theta}(\theta).\Theta_{nm}(\theta)\sin(\theta)\,d\theta\right)\left(\int_{\varphi=0}^{2\pi} M_{nm}^{\varphi}(\varphi).\Phi_{m}(\varphi)\,d\varphi\right) \neq 0 \tag{11a}$$

$$\left(\int_{\theta=0}^{\pi} M_{nm}^{\theta}(\theta).\Theta_{n'm'}(\theta)\sin(\theta)\,d\theta\right)\left(\int_{\varphi=0}^{2\pi} M_{nm}^{\varphi}(\varphi).\Phi_{m'}(\varphi)\,d\varphi\right) = 0, \ \forall (n',m') \neq (n,m) \tag{11b}$$

Each function M_{nm} has to maximize (11a) with respect to (11b). In (11b), one of the two integrals has to be zero to fulfill the condition.

1) Behavior of $\Theta_{n'm'}$

Let's suppose that the second integral in (11b) is not equal to zero. The study of the properties of $\Theta_{n'm'}$ allows canceling the first integral for some cases. Indeed, when the sum $n'+m'$ is even, functions

$Y_{n'm'}$ are symmetrical with respect to the equator plane (they are labeled with a black dot on Fig. 3). The others are anti-symmetrical. The sensor function M_{nm} should therefore have the same properties than the corresponding function Y_{nm}. Indeed, if it presents a symmetry with respect to the $z = 0$ plane, anti-symmetrical $\mathbf{B}_{n'm'}$ components will not create any disturbance flux, and vice versa. In the following, this principle will be chosen. Fig. 4 shows the case of component Y_{21} and the associated sensor geometry. At this step, there is no constraint on the opening angle θ_S. Thus, it is chosen as maximal ($\theta_S = \pi/2$ in M_{21} case on Fig. 4), what allows maximizing the signal for the flux created by $\mathbf{B}_{21}$.

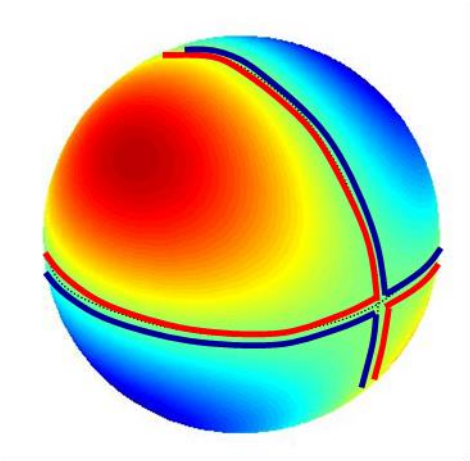

Fig. 4. Component Y_{21} and a first design for the associated detection coils shape M_{21}.

2) Behavior of $\Phi_{m'}$

The goal is now to cancel the second integral in (11b), the first one being possibly not equal to zero. According to the previous step, let us remember that for symmetrical sensors only symmetrical components have to be studied and inversely for anti-symmetrical ones.

The $\Phi_{m'}$ functions are m'-periodical. Therefore, functions M_{nm}^{φ} will also have this property as shown on Fig. 4. On this example, the opening angle φ_S of each coil is limited to the π/m maximal value. It remains now to evaluate the disturbance flux created in such coils by others components of the decomposition.

According to (11.b) and (7), we have:

$$Flux_{nm} \propto \int_{\varphi=0}^{2\pi} M_{nm}^{\varphi}(\varphi).\cos(m'\varphi).d\varphi \tag{12}$$

where the variations of M_{nm}^{φ} are shown on Fig. 5. We are in the well-known configuration of Fourier series decomposition where m' is equivalent to the signal pulsation. Thus:

- If $m' < m$, component $Y_{n'm'}$ do not create any disturbance flux. Indeed, the first non zero coefficient of the expansion corresponds to the fundamental of M_{nm}^{φ}.
- If $m' = m$, the integral in (12) is not zero.
- If $m' > m$, the only components $Y_{n'm'}$ creating a flux have a degree $m'=(2k+1)m$ (k integer). Indeed, for the $m = 1$ and $m = 2$ cases, we get:

For m=1: $\int_{\varphi=0}^{2\pi} M_{n1}^{\varphi}(\varphi).\cos(m'\varphi).d\varphi = \begin{cases} \frac{4}{m'}\sin(\frac{m'\varphi_S}{2}) & for\ odd\ m' \\ 0 & for\ even\ m' \end{cases}$ (13a) (13b)

For m=2:

$$\int_{\varphi=0}^{2\pi} M_{n2}^{\varphi}(\varphi).\cos(m'\varphi).d\varphi = \begin{cases} \frac{8}{m'}\sin(\frac{m'\varphi_S}{2}) & for\ m' = 2,6,10\ldots \\ 0 & for\ m' = 3,4,5,7,8,9\ldots \end{cases}$$ (13c) (13d)

In (13b) and (13d) the integral vanishes independently of sensor angle φ_S.

Finally, let us point out that for the *m = 0* cases, only the components of same degree *(m' = 0)* create a parasitic signal.

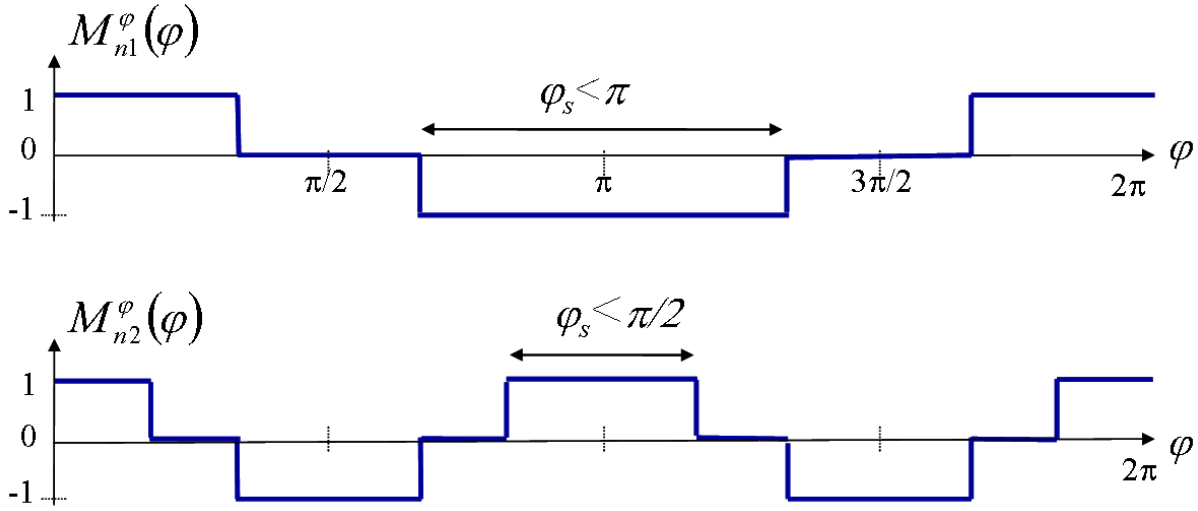

Fig. 5. M_{nm}^{φ} functions for *m = 1* and *m = 2* cases.

3) Influences

The previous results allow determining the table I. It shows elements Y_{nm} to be identified in blue, and those, which disturb their identification in red. At this step, constraints imposed on functions sensors are:

- the symmetry (on the right hand side) or the anti-symmetry (on the left hand side) in comparison with the equator plan *z = 0*,
- the periodicity linked to the degree of the searched component.

Fluxes have to be maximized; therefore, all opening angles φ_S and θ_s are chosen to get a maximal value by respecting these constraints. For example, concerning Y_{11} detection, only elements with an even (*n*+*m*) can disturb it; this corresponds to all those appearing in the left part of the table I. But, according to the M_{11} periodicity, only the elements of degree *m' = 3* remains. It corresponds to components Y_{31} and Y_{33}.

TABLE I. TABLE OF INFLUENCES FOR THE FIVE DIFFERENT SHAPES

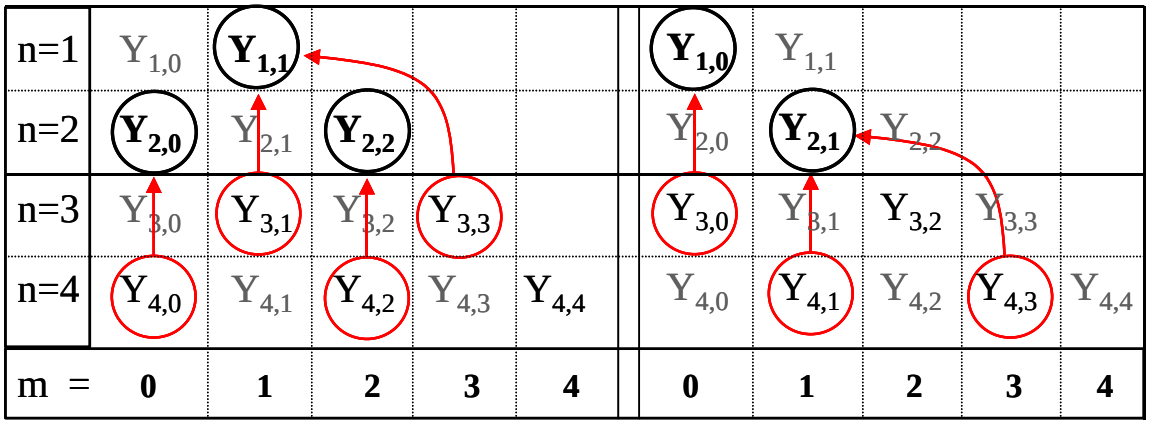

4) How to remove the last cross effects?

The last step consists in reducing the opening angles θ_S and φ_S in order to remove the last cross effects. However, it will lead to a decrease of the measured flux.

a) According to φ_S

Equation (13a) points out that it is possible to cancel the parasitic components whose index is a multiple of 3 by choosing $\varphi_S = 2\pi/3$. So, influences of Y_{33} on Y_{11} and of Y_{43} on Y_{21} disappear. It remains then only a single parasitic signature by aimed component.

b) According to θ_S

This opening angle can have values included between *0* and π. Two different cases lead to two different studies. For the case where functions M_{nm} are symmetrical, the only way to reduce them is to cut the coils from poles. The value of the angle, which cancels the disturbance component, is given by the solution of (14a). For the anti-symmetrical case, the cut must begin from the equator and the solution is given by (14b). Indeed, in both cases, the cancellation of the first integral in (11b) is achieved by looking when $M_{nm}^{\theta}(\theta) = 1$.

$$\int_{(\pi-\theta_S)/2}^{(\pi+\theta_S)/2} \Theta_{n'm'}(\theta).\sin(\theta).d\theta = 0 \quad (14a)$$

$$\int_{0}^{\theta_S} \Theta_{n'm'}(\theta).\sin(\theta).d\theta = 0 \quad (14b)$$

C. Example design of sensor M_{21}

To illustrate the proposed method, we focus on the design of function M_{21}. The complete process is shown on Fig. 6. At first, on the left, in accordance with parts *B.1.)* and *B.2.)*, a first basic shape is drawn. It fits at the same time the two previous constraints: the anti-symmetry with the *z = 0* plane and the periodicity on the azimuth of component Y_{21}. This design, with a smart composition, allows maximizing the fluxes in each coil (please take care to the winding way representing by blue and red colors). According to the table I, only elements Y_{41} and Y_{43} still disturb identification. In a second step, according to equation (8b), reducing $\varphi_S = 2\pi/3$ allows to cancel the effect of Y_{43}. It is shown on the

second sphere. Finally, on the right hand side, an angle, solution of equation (14b), exists, which allows to compensate exactly both lobes create by Y_{41}: $\theta_s = 1.35$ *rd.* According to notations of Fig. 6 (on the right) and after some algebra, (5) gives identification relation:

$$A_{21} = \frac{r_0^2}{1.7 \cdot 10^{-6}} . Flux_{21} \quad with \quad Flux_{21} = \left(flux_1 - flux_2 + flux_3 - flux_4 \right) \tag{15}$$

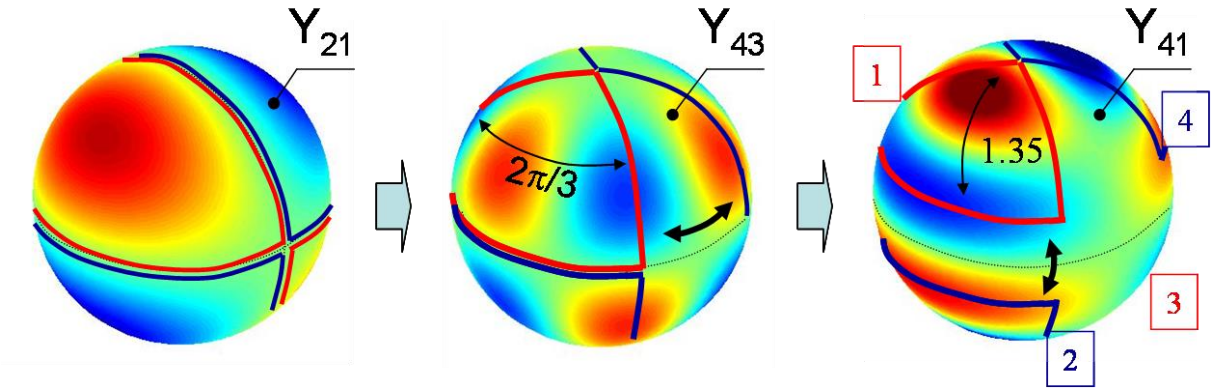

Fig. 6. Complete process for the sensor function M_{21} design.

The method is the same for designing all other sensors defined by functions M_{nm}. The obtained shapes are presented in table II of the appendix.

IV. Validation by the Finite Element Method (F.E.M.)

To validate the method, a toroidal inductor has been simulated (5 cm diameter - Fig. 7). It corresponds to the common mode filter of a variable speed drive. The aim is to determine the coefficients of the multipolar expansion. We have included the identification of the first and second order of the decomposition (all 8 sensors). The coefficients A_{1m} and A_{2m} have been identified at a distance of 10 cm from the inductor geometrical center. This distance is sufficient, with respect to the tore radius (2.5 cm), in order to keep valid the approximation of the reference source (limited at the fourth order).

All tests have been carried out in a finite element Software FLUX3D© [11], using a scalar magnetic potential formulation coupled with an infinite box transformation accounting for the external air region. The flux generated through the coils is computed using a post-processing surface integration.

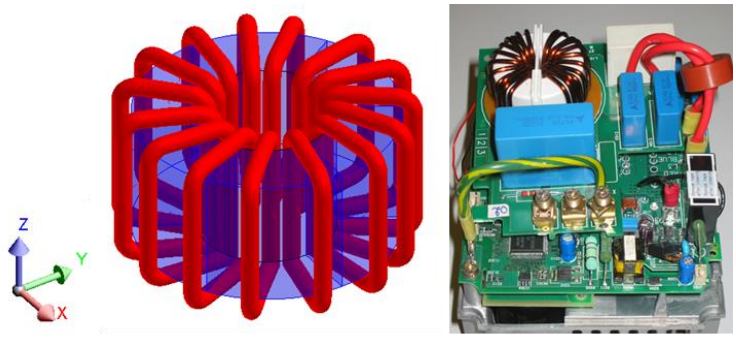

Fig. 7. Toroidal inductor and the associated variable speed drive.

A. Identification of A_{nm} and validation

After identification, Fig. 8 presents from 0.1 m to 2 m:

- the field obtained by the FEM,
- the reconstructed field including the first and second order terms,
- the reconstruction using the first order only,
- the reconstruction using the first order only, obtained by an identification following the Standard CISPR16-1.

The global behavior of all models is similar. However having a look at the relative error –with respect to the FEM solution- it can be seen that the first order is less accurate than the second order identification, close to the source. This was expected by the multipolar expansion theory. Furthermore, the first order identification obtained from the standard clearly shows that there was some inaccuracy in the dipole determination: it leads to about 13% of field error even far from the source. On the other hand, our sensors have determined the correct value, since far from the source, the field is well reconstructed.

The error in the determination of the dipole using the standard is due to the third order contribution in the sensor, according to table I. It is especially important since the identification has been carried out at a distance of 10 cm, where the high order components of the source have not decreased sufficiently.

The new sensor shape allows thus providing identification closer to the source than the standard (which recommends 1 meter). This is interesting since it brings more signal level and also reduces some propagation issues in the large coils.

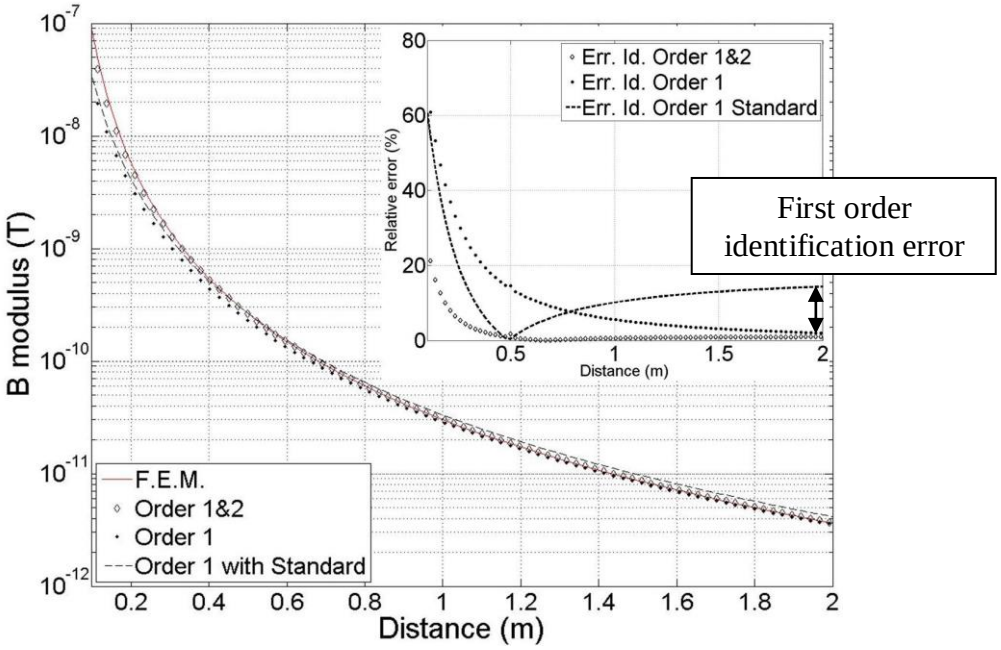

Fig. 8. Magnetic field decrease (modulus) vs the distance to the source: comparison between the identified dipole/quadrupole with the proposed and Standard sensors and the actual field, simulated by the FEM.

B. Identification and robustness

First, we check the robustness of the sensor to a change of sensor radius r_0: three different sensors for three different measurement distances have been tested, the identification has been found very stable (less then 1% error on the identification). It confirms that it is not necessary to be far from the source to identify the dipole and quadrupole, contrary to the standard solution [4]-[6].

The second verification concerns a mismatch between the inductance center with respect to the decomposition center. This implies a more complex field (i.e. higher orders in the decomposition) [9]. Only dipole identification is concern by this phase. The results of the FEM simulation show that an error on the dipole determination occurs (Fig.9). It is due to the contribution of B_{5m} (and higher orders) terms in our sensor. However, the error is reasonable, and lower than using the Standard antenna, since this latter is sensitive starting from B_{3m}.

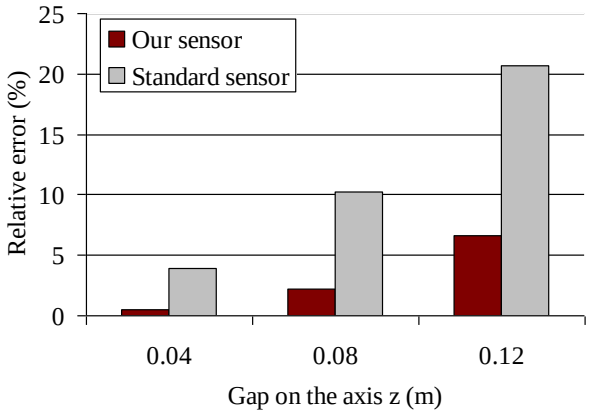

Fig. 9. Comparison between Standard antenna and the proposed sensor for a shifting source: relative error of the dipole identification compared to the actual dipole. The dipole computation is achieved by summing the three components of the dipole: $\sqrt{A_{10}^2 + A_{11}^2 + A_{1-1}^2}$

V. CONCLUSION

The multipolar expansion is attractive to synthesize a magnetic field because it provides accuracy with only few parameters. To identify the components of the decomposition, it seems not convenient to use several punctual measurements. Therefore, we choose to develop dedicated sensors, sensitive to a specific component of the expansion only. These coils have been designed, with special shapes, until the second order of the decomposition. The validation of all sensors has been carried out using a finite element software.

Thus, we have shown that Standard sensor could be improved. Indeed, on the one hand, our sensors do not create identification error when the radius decreases. On the other hand, they are more robust when dipole shifts from the system center. Furthermore, we have shown that it could be possible and interesting to design sensors which also identify the quadrupole components by filtering exactly the components of orders 3 and 4.

The construction of the sensors is in progress, and experimental results will be given in future papers. Nevertheless, the construction of the complete system is still complex. We have restrained the

sensor design with constant θ or φ angles. Without these constraints, other geometrical properties of Y_{nm} lead to the same identification with only two different shapes of sensor: future works will expose these developments.

APPENDIX

TABLE II. SHAPE OF THE SENSORS

<table>
<tr><th></th><th>n = 1</th><th colspan="2">n = 2</th></tr>
<tr><td rowspan="2">m = 0</td><td> 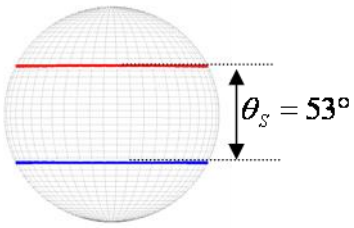
</td><td colspan="2"> 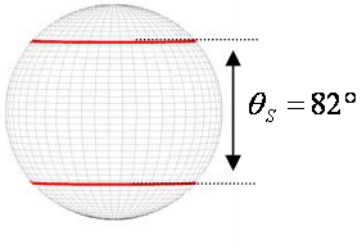
</td></tr>
<tr><td>$A_{10} = \frac{125 \cdot r_0}{4\pi \cdot 10^{-5}} Flux_{10}$</td><td colspan="2">$A_{20} = \frac{r_0^2}{7.0514 \cdot 10^{-7}} Flux_{20}$</td></tr>
<tr><td rowspan="2">m = +/-1</td><td rowspan="2"> 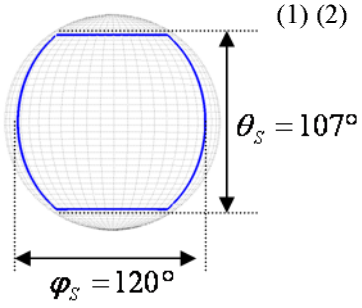
</td><td>View on x axis (1) (2)</td><td>View on z axis</td></tr>
<tr><td> 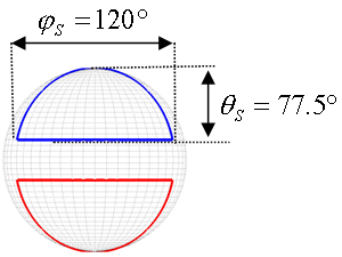

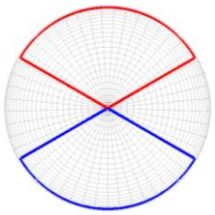 </td></tr>
<tr><td rowspan="2">m = +/-2</td><td rowspan="2">(1) Same shape in the opposite side,
(2) for $m < 0$, sensors are rotated by
$\varphi = \frac{\pi}{2m}$</td><td colspan="2"> 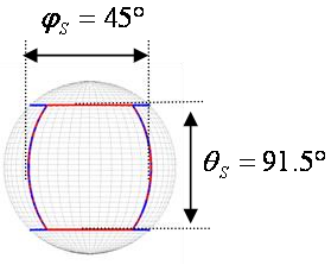

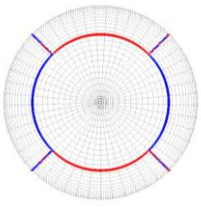 </td></tr>
<tr><td colspan="2">$A_{22} = \frac{r_0^2}{1.2344 \cdot 10^{-6}} Flux_{22}$</td></tr>
<tr><td>$A_{11} = \frac{-r_0}{9.7822 \cdot 10^{-7}} Flux_{11}$</td><td colspan="2">$A_{21} = \frac{-r_0^2}{1.1147 \cdot 10^{-6}} Flux_{21}$</td></tr>
</table>

ACKNOWLEDGMENT

This work was supported in part by the CAPES-COFECUB (project 568/07) and the FAPESP (project 2008/53611-9).

REFERENCES

[1] J.P. Keradec, J. Lorange, J.-L. Schanen, B. Cogitore, T. Creuzet, C. Brun, "Nano-teslameter for characterization of the fields emitted and received by wound electronic components," IMTC 2003.
[2] L.-L. Rouve, L. Schmerber, O. Chadebec, A. Foggia, "Optimal magnetic sensor location for spherical harmonic identification applied to radiated electrical devices," Magnetics, IEEE Transactions on, Volume 42, Issue 4, April 2006 pp. 1167-1170
[3] A.V. Kildishev, S.A. Volokhov, J.D. Saltykov, "Measurement of the Spacecraft Main Magnetic Parameters," IEEE, 1997, pp. 669-675.
[4] J.R. Bergervoet and H. Van Veen, "A large-loop antenna for magnetic field measurements," Zurick International Symposium on EMC, Proceedings, 1989, pp.:29-34.
[5] M. Savi, T.Z. Gireli, F.A. Tirich, C. A. F. Sartori, "Developing a Van Veen & Bergervoet Antenna," EMC 2004, pp. 717-720.
[6] Standard CISPR 16-1, annex P, 2002, pp. 230-237 and 396-409.
[7] W. A. Pasmooij, "A 'Helmholtz' large loop antenna system for improved magnetic field measurements," EMC 1992, pp. 143-148.
[8] J.D. Jackson, "Classical Electrodynamics," 3rd ed., 1998, pp.407-456.
[9] J.P. Wikswo, "Scalar multipole expansions and their dipole equivalents," J. Appl. Phys., 1985, pp. 4301-4308.
[10] J.C. Nedelec, "Acoustic and electromagnetic equations: integral representations for harmonic problem," Springer, 2001, pp. 24.
[11] http://www.cedrat-groupe.com/